IOPscience iopscience.iop.org

Home Search Collections Journals About Contact us My IOPscience

Electron optical aspects of the dual-emission electron spectromicroscope

This article has been downloaded from IOPscience. Please scroll down to see the full text article.

2005 J. Phys.: Condens. Matter 17 S1351

(http://iopscience.iop.org/0953-8984/17/16/006)

View the table of contents for this issue, or go to the journal homepage for more

Download details:
IP Address: 129.252.86.83
The article was downloaded on 27/05/2010 at 20:39

Please note that terms and conditions apply.

INSTITUTE OF PHYSICS PUBLISHING JOURNAL OF PHYSICS: CONDENSED MATTER

J. Phys.: Condens. Matter **17** (2005) S1351–S1362 doi:10.1088/0953-8984/17/16/006

Electron optical aspects of the dual-emission electron spectromicroscope

Krzysztof Grzelakowski

Opticon, Uznamska 8, PL54-315 Wroclaw, Poland

Received 9 December 2004, in final form 9 December 2004
Published 8 April 2005
Online at stacks.iop.org/JPhysCM/17/S1351

Abstract
The electron optical configuration of the novel dual-emission electron spectromicroscope (DEEM) is discussed. The idea of DEEM is based on the concept of the double deflection of the electron beam, initially by the angle $+\alpha$, through the first concentric spherical deflector and then, after passing through the relay lens, by the angle $-\alpha$ through the second concentric spherical deflector. That novel concept allows parallel observation at two independent imaging units of two different electron optical images: the unfiltered real image and energy filtered electron angular distribution or electron angular distribution and the energy filtered real image. The dispersion of the first deflector lens system is used for the selection of the energy range of the emitted electrons. The relay lens reverses the sign of the distance from the electron optical axis and the angle to this axis of the electron at the input to the second deflector, leading in the ideal case (C_c and C_s equal to 0) to the cancellation of the chromatic and spherical aberrations in the output image plane of the deflector system.

It will be also shown that DEEM instrumentation allows high energy electron sample illumination, which opens new possibilities for chemical mapping and analysis (ESCA, Auger) on a nanometric scale under laboratory conditions.

1. Introduction

The complete understanding and control of complex processes and materials on the nanometric scale requires usage of advanced research techniques and instruments. Growing miniaturization and compactness of structured systems demands not only sufficient lateral resolving power of those instruments but also their ability to supply the local electronic and magnetic information. One way of realizing this goal might be through combination of the traditional emission electron microscope with an imaging energy filtering system [1–3]. The emission microscope does not scan an electron beam over the sample. Instead, the sample is evenly illuminated with electrons, photons or ions, which results in plurality of contrast

mechanisms [4, 5]. These contrast mechanisms contribute to simultaneous visualization of object points, allowing in real time for observation and investigation of dynamic processes at surfaces [6].

In the case of illumination with a laboratory UV light source, excitation of photoelectrons from the valence band occurs, allowing only work function contrast. This limitation can be overcome with high energy synchrotron radiation [7] or by illumination with high energy electrons, as will be described below.

2. General description of the instrument

The dual-emission electron microscope is a fully electrostatic instrument that consists of five main segments: the immersion objective with a manipulator, the electron retarding unit for increasing the energy resolution, the double-spherical-deflector unit with a relay lens in between the deflectors and two independent parallel columns with two MCP imaging units [8]. The principle of the idea is shown schematically in figure 1. Since figure 1 has been taken generally from the patent application [8], all lenses and other electron optical elements are drawn schematically, and will be described in more detail below. The first electron optical part is a tetrode immersion objective (1), which consists of a sample (2) and three electrostatic electrodes [9, 10]. The sample cartridge is held in the X–Y piezo-quartz driven manipulator (3), which is mechanically fixed to the objective to minimize vibrations and to simplify the assembling of the system [11].

One of the most important aspects of emission microscopy is the kind and energy of the illumination of the sample [5]. For the spectroscopic applications of DEEM it is very important to be able to excite the core level electrons in the analysed sample. There are many examples of the usage of synchrotron radiation in such experiments [7].

One of the important goals of the development presented here is achieving the possibility of a chemical analysis of different samples under laboratory conditions. This motivation has led to the development of a novel method of sample illumination [8], which will be described in section 3, and is shown schematically in figure 1. The miniature electron gun (4a) is brought close to the electron optical axis. As indicated in figure 1, in order to come closer to the axis and save space, miniature, concentric curved deflector plates were used (4b). The injection of the electrons is done at an angle of about 2.5° which results in an illumination angle at the sample of about 6°–10°, depending on the negative potential of the cathode of the electron gun, which varies between −2 and −5 kV. As a consequence, the central area of the sample, which is kept close to the ground potential, is illuminated by electrons having sufficient energy (2–5 keV) for excitation of core level electrons and emission of Auger electrons used for chemical selective imaging of a sample. The electron optical aspects of the high energy sample illumination will be described in section 3.

The expected energy range of secondary, Auger and inelastically scattered electrons emitted from the sample is close (with respect to the work function difference between sample and cathode) to the energy of the primary beam. For that reason, in order to reduce the impact of chromatic aberrations of the objective on the lateral resolution, it is particularly important to be able to select a narrow energy band for use in the imaging process.

This is done in DEEM by means of two spherical and opposite deflectors, separated by the relay lens [8]. The inner and outer spherical electrodes are precisely separated at their ends by two ring electrodes (14) interleaved with sapphire insulators.

Although the chromatic aberrations of the deflector system, caused mainly by the relay lens (15), are higher than the chromatic aberrations of the objective, the energy selection done by the deflector system leads to a huge improvement of the total lateral resolution.

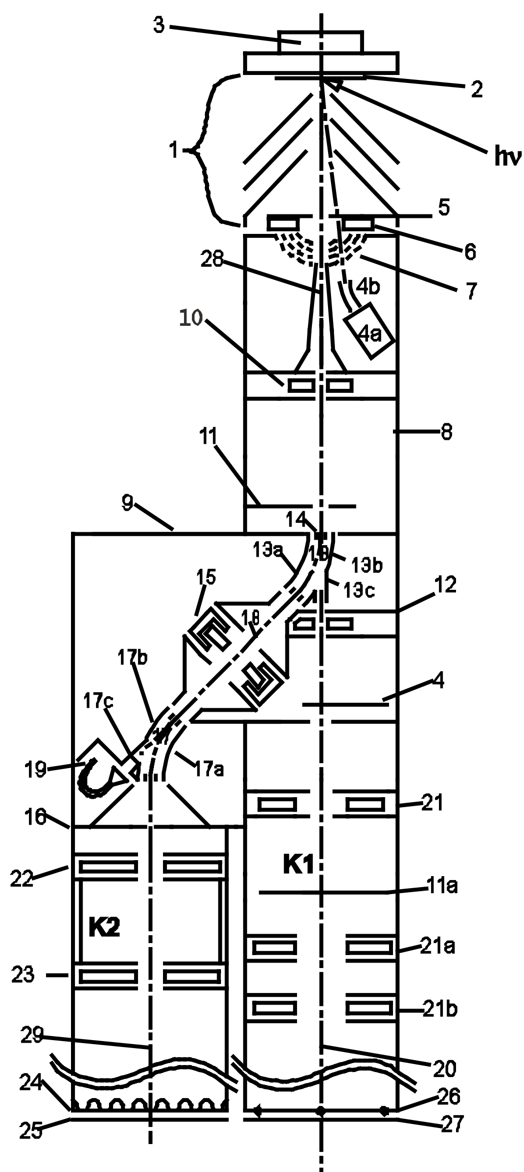

Figure 1. A schematic illustration of the electron optical system (not to scale): (1)—cathode objective lens, (2)—sample, (3)—sample manipulator, (4)—contrast aperture, (4a)—electron source, (4b)—spherical deflector, (5)—objective focal plane, (6)—stigmator, (7)—radial retardation system, (8)—objective tube, (9)—electrostatic shield, (10, 12, 21, 21a, 21b, 22, 23)—einzel lenses, (11, 11a)—field apertures, (13)—first spherical deflector, (14)—fringing field corrector, (15)—relay lens, (16)—aperture, (17)—second spherical deflector, (18)—dispersion aperture, (19)—channeltron, (20, 29)—electron optical axis of the imaging columns, (24, 25 and 26, 27)—image intensifiers, (28)—electron optical axis of the cathode objective lens, (K1)—first imaging column, (K2)—second imaging column.

The first deflector lens system (13) with the deflection angle of $+\alpha$ is used as an energy analyser for the selection of the energy range of the emitted electrons. The outer electrode of the second deflector (17) has a bore in order to enable electrons to drift towards the channeltron (19).

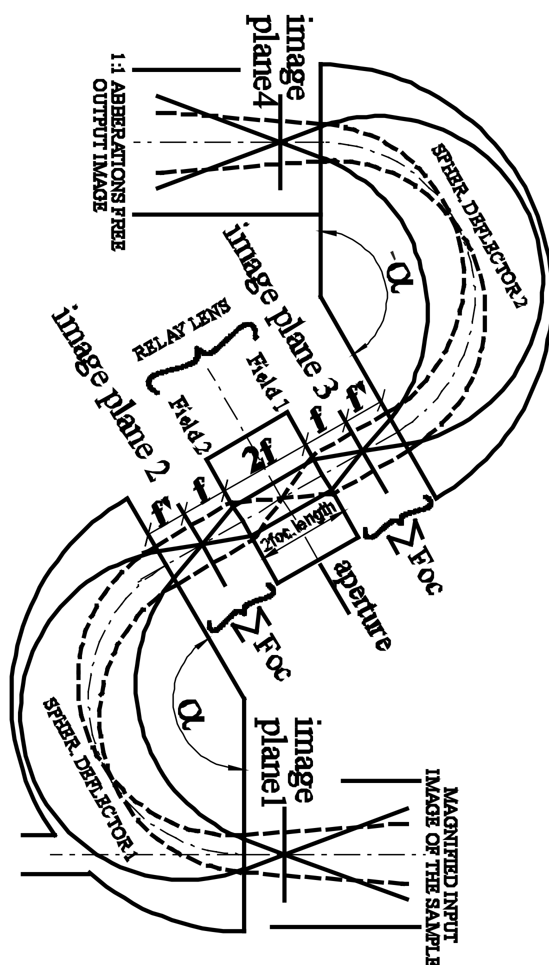

Figure 2. The imaging deflection/filtering system with two opposite concentric spherical deflectors and a relay lens. (f' and f denote the focal distances of the spherical deflector and the relay lens, respectively.)

The only function of the relay lens is the transformation of the image from the output of the first deflector to the input of the second deflector in 1:1 correspondence, with the following requirements: $T(\mathbf{r}) = -\mathbf{r}$ and $T(\beta) = -\beta$ (where T denotes the electron optical action of the lens, $\mathbf{r}$ is a vector describing the distance from the axis and β is a slope). The second spherical deflector, with the deflection angle of $-\alpha$, then transfers this reciprocal image (simultaneously cancelling all aberrations) to the input of the imaging column. The optimal function can be achieved only (in any case of general deflection angle α) when the deflectors are separated exactly by twice the value of the focal lengths of the deflector (f') and the relay lens (f) (figure 2) [8]. It will be analytically shown in section 4, for one of the possible deflection angles: $\alpha = 180°$ (hemispherical analyser), that in the case of an ideal relay lens (C_c and C_s equal to 0) the idea leads to the total cancellation of the chromatic and spherical aberrations of the deflector system and an aberration free image appears at the output of the second spherical deflector. Such cancellation of aberrations takes place for any deflection angle α, provided that the separation equals twice the value of the focal lengths (figure 2). In section 4 a real

relay lens, with chromatic and spherical aberrations C_c, C_s differing from zero, will also be considered. The non-zero aberrations of the relay lens result in a worsening of the lateral resolution. The worsening of the lateral resolution is directly proportional to C_c for the relay lens, while the influence of C_s on the image quality is negligible due to the very small opening angles.

Since the dispersive action of the first spherical deflector is used for the energy analysis, we can apply well known formulae for the spherical analyser [12]. It is easy to show that the energy resolving power of the spherical analyser is inversely proportional to the pass energy. For that reason, it is important to be able to lower the kinetic energy of electrons before entrance to the first deflector, without worsening the lateral resolution. This can be achieved by applying a retarding central force field with the field centre located exactly at the contrast aperture [8]. This idea will be presented in a more detailed way in section 5.

3. The method of high energy electron sample illumination

For the electron illumination of the sample we apply a miniature electron Auger gun, with the capability of producing primary electrons with energy up to 5 keV [13]. The electron gun consists of three segments: a spherical deflector unit (4b, figure 1), an objective lens and a CeB_6 cathode, Wehnelt and anode. All electron optical elements, with the exception of the Wehnelt, are made of titanium. The Wehnelt electrode, because of the high temperature requirement, is constructed of molybdenum. The outer diameter of the gun is constrained to 10 mm in order to fit inside the shield tube, which is kept at microscope potential to ensure a field free space around the gun. After some improvement, the gun permits operation at up to 5 kV. An emission current of about 150 μA can be obtained in the telescopic mode of operation.

For the application goal, the gun described above has been equipped with a 30° spherical deflector (4b, figure 1). It allows bringing the primary electrons closer to the axis (2.5°) and increases the distance between the electron optical axis and LaB_6 cathode of the gun, which is important because of the stray magnetic field due to the heating current. Since the requirements for the spot quality in the Auger mode are much weaker than in LEEM instruments [6], one can run the gun in nearly telescopic mode, at high emission currents (0.15 mA). The focusing of the primary beam takes place in the decelerating field between the extractor electrode and sample. The resulting spot size at the sample is about 300 μm.

Figure 3 illustrates the trajectories of primary and secondary electrons calculated by SIMION 6.0 [14] using typical, experimental values: primary energy 2.5 keV, secondary energy 300 eV (Auger peak energy), extractor voltage 15 kV, focus electrode voltage 700 V and drift potential (last electrode) 1200 V. The energy spectrum of the electrons can be measured by means of the channeltron (19) by fixing the energy window of the analyser (fixed pass energy) and changing the potential of the sample (2). Since the contribution of the sample potential to the total extractor field is small, only negligible shift of the primary electron beam is expected. In the case of larger energy ranges this shift can be compensated by correction to the spherical deflector (4b) in the gun using computer software.

4. The double-spherical-deflector–lens system

A qualitative illustration of the imaging analyser for a general deflection angle α [8] is given in figure 2. The behaviour of the α and γ rays clearly demonstrates the idea of combining the two spherical deflectors separated by the relay lens. Two α rays starting from the point on the axis at the input of the first deflector are crossing again at the output of deflector, although slightly

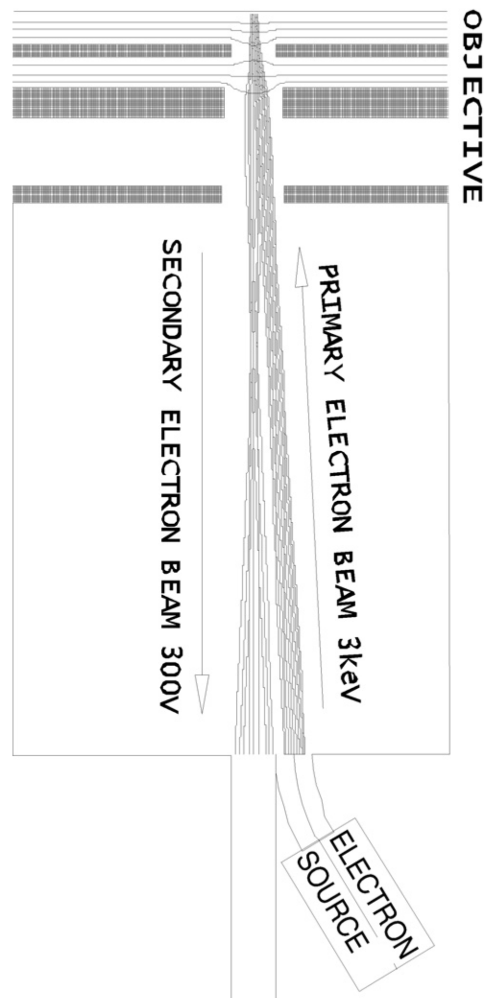

Figure 3. An electron optical illustration of the idea of the high energy electron beam sample illumination through the cathode lens.

off the axis. The relay lens transfers this point with reversed sign and slope (by refracting α rays at electron optically equivalent refraction planes F1 and F2 of the relay lens; figure 2) to the input of the second deflector.

For symmetry reasons, that point is transferred again to the axis, but only when the separation is equal to double the value of the focal lengths (f', f) of the electron optical elements [8], as indicated in figure 2. As a consequence, for the same symmetry reasons, the relay lens has to be constructed in such a way that its refraction planes F1 and F2 have to also be separated by double the value of the focal length (f). Bringing two deflectors closer or moving them further than double the value of the focal lengths (f', f) would result in breaking of the symmetry and degrading of the cancellation of aberrations.

In order to perform exact analytical calculations for such a complex unit (two opposite, spherical analysers and a relay lens between them), an ideal model of the system has been assumed. Firstly, at the edges of the deflectors there is an abrupt (step-like) change of an ideal spherical potential distribution to the constant value outside (field free area), and secondly the

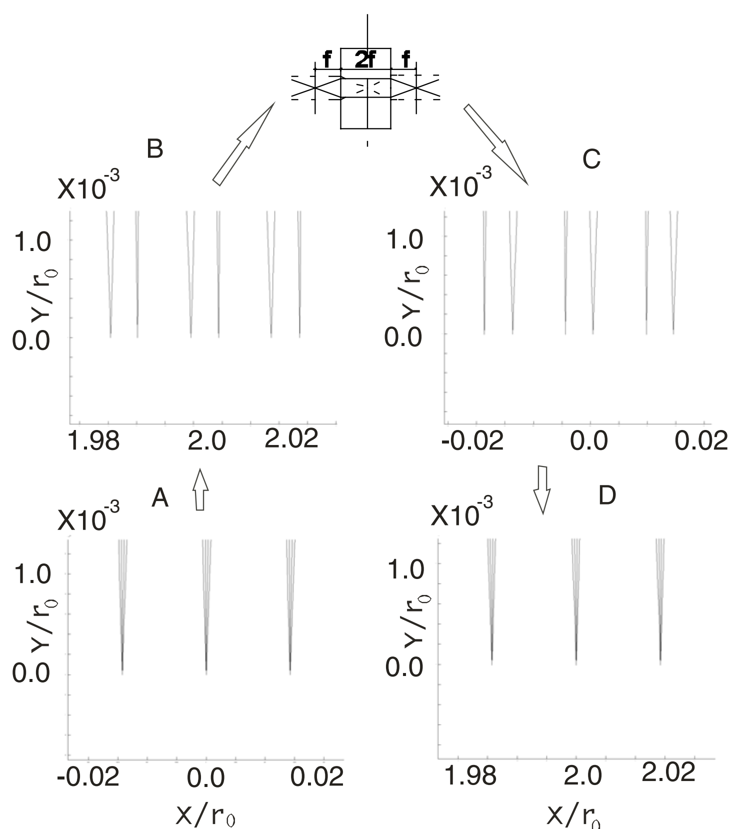

Figure 4. Calculated electron beam trajectories inside the concentric spherical deflectors at the edges: $\Delta E/E = 0$, $\Delta\beta = 3°$, C_c and C_s for the relay lens equal to 0. (A) and (B)—input and output of the first deflector, respectively. (C) and (D)—input and output of the second deflector, respectively.

object at the input is represented by a set of perfect pencils having point crossovers. For further illustration, a special case of the concept, $\alpha = 180°$, was chosen (two hemispheres with a relay lens between them).

The assumptions above allow us to take the exact analytical solution of the second-order differential equation of motion for electrons crossing the step-like (ideal) edge of the spherical potential distribution. The trajectories of electrons are then perfect Kepler orbits of different sizes and forms, depending on the input energy and angle.

Let us consider trajectories of electrons in the normalized Cartesian coordinates x/r_0, y/r_0 ($r_0 = (r_1 + r_2)/2$, where r_1 and r_2 are the inner and outer radius, respectively, and x, y describe distances from the central point at the input to the deflector), when the zero orbit has a radius equal to 1, focal properties of the relay lens do not depend on the energy or the angle (C_c, $C_s = 0$) and the α ray bundle angular spread $\Delta\beta$ and the normalized energy spread $\Delta E/E$ are equal to 3° and 0, respectively.

Figure 4 illustrates the above situation, when the kinetic energy of the electrons in the α ray bundle is equal to the pass energy of the hemispherical deflectors. The perfect set of three point pencils, separated by a distance of 0.014 at the input of the first deflector (figure 4(A)), smears out to 0.005 at its output (figure 4(B)). The lateral resolution at the sample (assuming

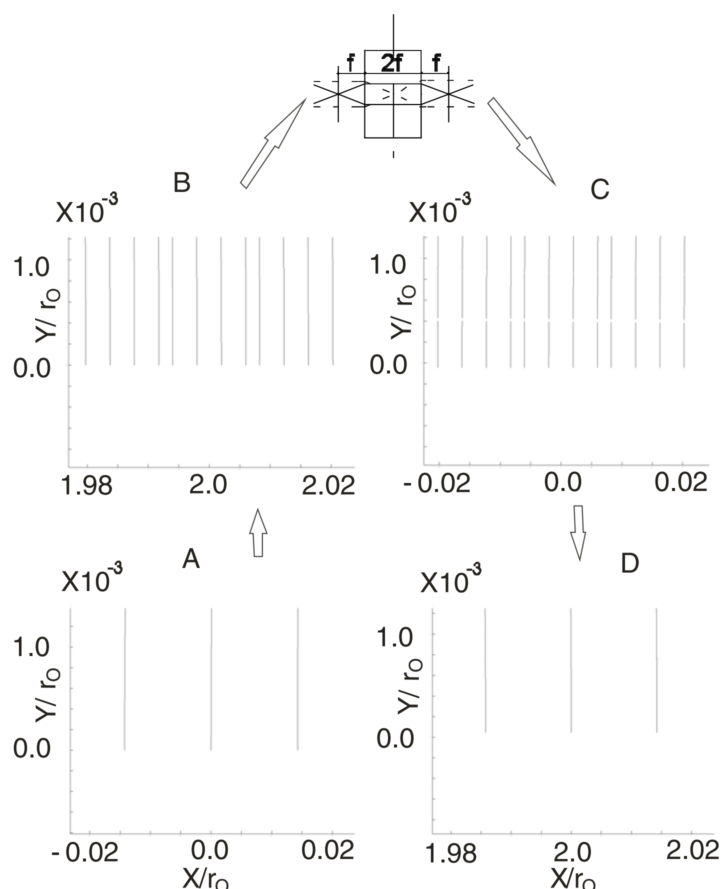

Figure 5. Calculated electron beam trajectories inside the concentric spherical deflectors at the edges: $\Delta E/E = 0.002$, $\Delta\beta = 0°$, C_c and C_s for the relay lens are equal to 0. (A) and (B)—input and output of the first deflector, respectively. (C) and (D)—input and output of the second deflector, respectively.

$r = 100$ mm and objective magnification $M = 50$) is equal to 10 μm. This value is much too high to be useful for imaging purposes. The switching of the relay lens described above leads only to reversal of the phase and the positions of α rays, without improving the quality of the image, as seen in figure 4(C). Finally, applying the electron optical action of the second deflector with $-\alpha$ deflection causes complete cancellation of spherical aberrations. The set of three output pencils is illustrated in figure 4(D). In the case of an ideal relay lens (no aberrations), a perfect one-to-one copy of the input set of pencils from figure 4(A) is obtained at the output.

The same calculations have been repeated with the energy of the electrons smeared out around the pass energy by $\Delta E/E = 0.002$ and the angular spread $\Delta\beta$ equal to 0°.

Figure 5 shows the result at different stages of the deflector unit. Figure 5(A) illustrates three γ rays, each of them built of four rays at different energies. Passing through the first deflector results in a separation over energy—the highest separation appears at the output of the deflector; figure 5(B). For that reason the output plane (or equivalently the input plane of the second deflector) could be treated as the most suitable choice for the location of the

dispersion aperture. But more careful study of this dispersion plane shows that the location of energetically separated rays depends on the position of the starting point of electrons along the field vector, which corresponds to the shift at the sample along the line, in the plane of deflection. The fixed slot aperture in one of these two equivalent planes acts as an upper cut-off filter for one side of an image and as a lower cut-off filter for another one. Only the middle part of the image is transferred in a correct way, symmetrical in energy. Alternatively one can use the field free area in the centre of the relay lens for the energy analysis, although the dispersion is low at that plane. In the field free centre of the relay lens, as seen in figure 2, the crossover of γ rays appears. This allows for a much smaller aperture than at the output of the analyser, without reducing the opening angles of pencils and therefore the intensity.

The electron optical action of the relay lens is identical to the previous case. Reversal of the phase and the position occurs and the reciprocal but still energetically smeared image appears at the input of the second deflector (figure 5(C)). Due to symmetry, all energetically separated rays are perfectly brought together at the output of the second deflector, as seen in figure 5(D).

The above consideration has been carried out under the assumption that the spherical and chromatic aberrations of the relay lens are equal to zero. In that case, as has been shown above, the whole three-element deflection system (two hemispheres and the relay lens between them) acts as a completely aberration free imaging unit.

Let us consider a more realistic situation, where the refraction planes F1 (field 1) and F2 (field 2) of the relay lens in figure 2 introduce into the system their own aberrations. We have built our lens on the basis of the ideas presented in the paper by Rempfer [15]. The chosen lens had the following parameters: $t/D = 1.0$; $s/D = 0.4$; $V_L/V_C = 0.8$, where s denotes interelectrode spacing, t and D are the thickness and diameter of the centre electrode and V_L and V_C are the potentials of the centre electrode and cathode, respectively. Since the relay lens has to be symmetrical, the chromatic and spherical aberration coefficients are identical for F1 and F2. The non-zero aberrations cause deviations in α and γ rays, at the refraction planes F1 and F2, depending on the energy and the angle, which results in an error in the image reversing process: $F(\mathbf{r}) = -\mathbf{r} + \Delta\mathbf{r}$ and $F(\beta) = -\beta + \Delta\beta$. Taking $\Delta\mathbf{r}$ and $\Delta\beta$ into account, we can calculate the new, disturbed α and γ rays. As seen in figure 6, total cancellation of the aberrations in the system is not possible any more, due to symmetry breaking, which takes place in the relay lens. The crossover of the γ rays for different energies appears then in the middle of the relay lens, but off the axis. For that reason, it is not possible any more to bring the rays again to a perfect point. Figure 6(A) shows the three perfect pencils of α rays, which have four different energies from the region of $\Delta E/E = 0.002$ and three angles: $-1°$, $0°$ and $1°$. After coming through the first deflector, γ rays smear like in the earlier case, as shown in figure 6(B). But now the relay lens, in the presence of aberrations, transfers this smeared set of rays to $-\mathbf{r} + \Delta\mathbf{r}$ and $-\beta + \Delta\beta$. This is why the aberrations of the first deflector cannot be fully cancelled by the second one. This can be seen in figure 6(C), which illustrates small, non-symmetrical changes in the γ rays caused by aberrations of the relay lens. The partial cancellation of the aberrations in the second deflector results in huge improvements of the lateral resolution at the output, as compared to the image output of the first deflector. If the same experimental parameters as in the ideal case are applied to realistic experimental conditions, the resulting lateral resolution is estimated to be 40 nm.

5. The retarding central force field

The energy resolving power of the double-deflector energy analyser is limited by the minimal possible size of the dispersion aperture. The dispersion aperture size is determined by the size

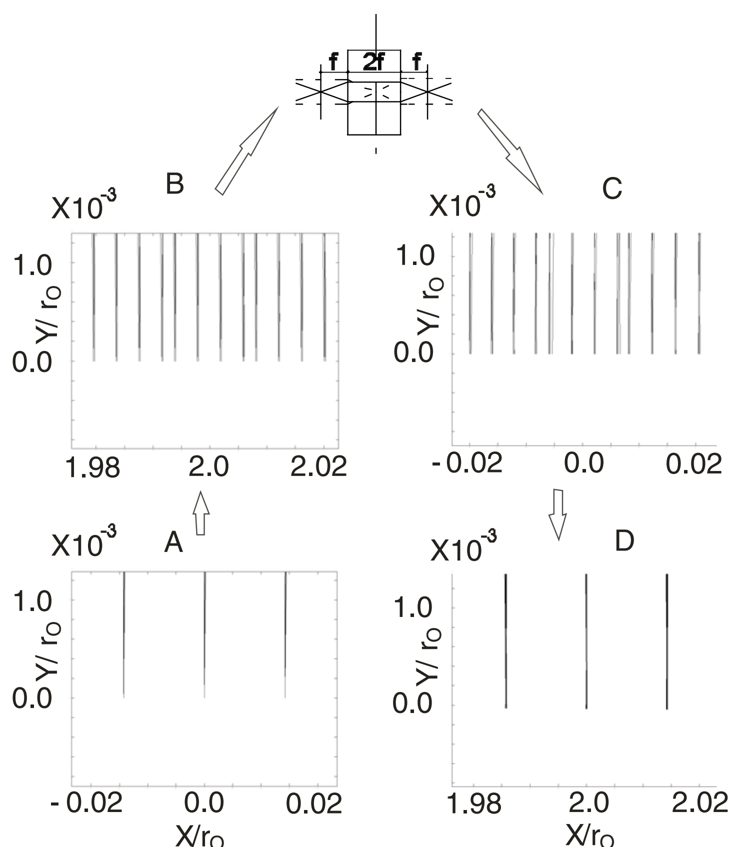

Figure 6. Calculated electron beam trajectories inside the concentric spherical deflectors at the edges: $\Delta E/E = 0.002$, $\Delta\beta = 2°$, C_c and C_s for the relay lens are equal to 3 and 9 [15], respectively. (A) and (B)—input and output of the first deflector, respectively. (C) and (D)—input and output of the second deflector, respectively.

of the smallest field of view (in the case of location in the image plane), or by the smallest contrast aperture size (in the case of location in the centre of the relay lens).

A further improvement can be obtained if the pass energy of the analysed electrons is lowered. In the case of conventional spectrometers the lateral information is not conserved and the deceleration of electrons is routinely achieved by means of a set of input lenses [16].

Since the DEEM is an imaging spectrometer, the conservation of lateral information is a fundamental goal [17]. The idea of the central force field retarding under the above requirement arises from the observation that the contrast aperture size is of the order of several micrometres and can be treated as a quasi-point source of electrons, since the image size is usually more than 100 times larger.

This fact is illustrated in figure 7(A). Locating the centre of the central force field simulated by a number of electrodes exactly at the contrast aperture allows the retarding of α rays along the field lines. The finite size of the aperture and conservation of the angular momentum result in bending of the trajectories. By utilizing this effect, with the focusing property of the objective, it is possible to get crossovers of α rays exactly at the image plane. The relationship between the distance from the axis at the diffraction plane and the distance from the axis in the imaging plane for different energies is shown in figure 7(B). By taking an energy spread

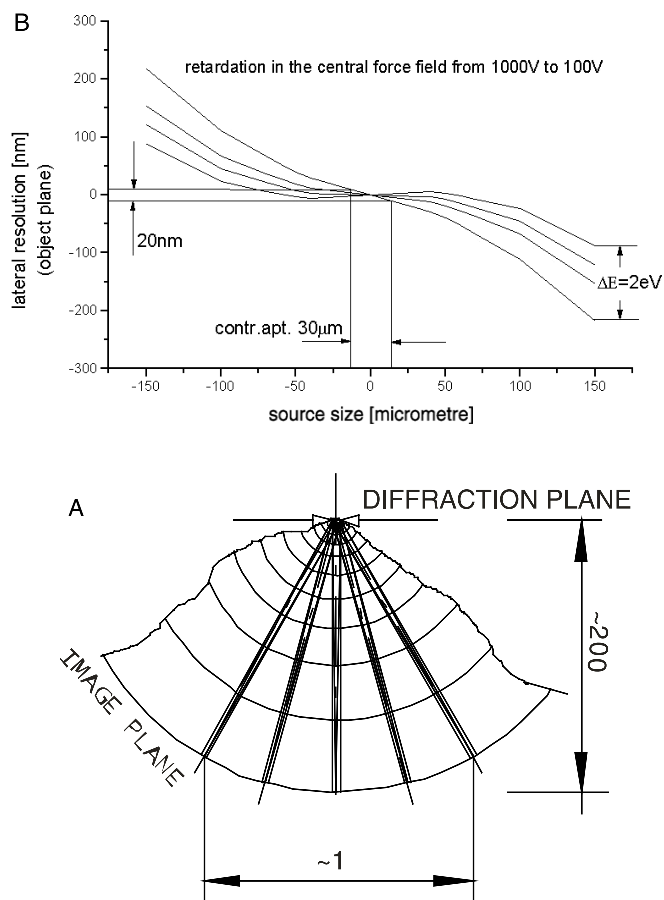

Figure 7. The method used for the retarding of electrons in cathode lens instruments: (A)—schematic illustration of the idea; (B)—distance of the electron from the electron optical axis in the imaging plane as a function of its starting position in the back focal plane for $\Delta E = 2$ eV at $E = 1000$ eV at that plane, after deceleration by a factor of ten.

of 2 eV, an aperture size of 30 μm and tenfold retardation, worsening of lateral resolution to 20 nm is expected. Simultaneously, the energy resolution is improved by a factor of ten.

6. Conclusions

Three of the most important electron optical aspects of the double-emission electron spectromicroscope were discussed. A detailed description of the DEEM was presented. The estimated theoretical value of the total lateral resolution can be obtained by taking into account the individual contributions of the retarding unit and the deflector system, which are 20 and 40 nm, respectively. The theoretical lateral resolution of the objective for the chosen kinetic energy of 200 eV is equal to 10 nm. The total lateral resolution in the spectromicroscopic mode is then below 50 nm with an expected energy resolution of about 100 meV.

Acknowledgments

My thanks are due to Janusz Krajniak for his support and help and to Piotr Zawadzki for reading the manuscript and discussions.

References

[1] Tonner B P *et al* 1997 *J. Electron Spectrosc. Relat. Phenom.* **84** 211
[2] Veneklasen L H 1991 *Ultramicroscopy* **36** 76
[3] Schmidt Th *et al* 1998 *Surf. Rev. Lett.* **5** 1287
[4] Doyle B L *et al* 1999 *Nucl. Instrum. Methods* B **158** 6
[5] Bauer E *et al* 1997 *J. Electron Spectrosc. Relat. Phenom.* **84** 201–9
[6] Telieps W 1983 *Dissertation* TU Clausthal
[7] Günther S *et al* 2002 *Prog. Surf. Sci.* **70** 187–260
[8] Grzelakowski K 2000 *International Patent Appl.* P.338538 (Poland)
Grzelakowski K 2003 *US Patent Specification* 6,667,477 B2
[9] Orloff J and Swanson L W 1979 *J. Appl. Phys.* **50** 2494
[10] Chmelik J, Veneklasen L and Marx G 1989 *Optik* **83** 155
[11] Grzelakowski K and Bauer E 1996 *Rev. Sci. Instrum.* **67** 742
[12] Purcell E M 1938 *Phys. Rev.* **54** 8
[13] Grzelakowski K, Man K L and Altman M S 2001 *Rev. Sci. Instrum.* **72** 3362
[14] Dahl D A, Delmore J E and Appelhans A D 1990 *Rev. Sci. Instrum.* **61** 607
[15] Rempfer G 1985 *J. Appl. Phys.* **57** 2385
[16] Seah M P and Smith G C 1990 *Surf. Interface Anal.* **15** 751
[17] Grzelakowski K 2004 *Surf. Sci.* **566–568** 869